ISSN 1063-7834, Physics of the Solid State, 2020, Vol. 62, No. 11, pp. 2167–2172. © Pleiades Publishing, Ltd., 2020.
Russian Text © The Author(s), 2020, published in Fizika Tverdogo Tela, 2020, Vol. 62, No. 11, pp. 1919–1924.

LOW-DIMENSIONAL SYSTEMS

The Composition and Magnetic Structure of Fe_3O_4/γ-Fe_2O_3 Core-Shell Nanocomposites under External Magnetic Field: Mössbauer Study (Part II)

A. S. Kamzin[a, *], I. M. Obaidat[b], A. A. Valliulin[c], V. G. Semenov[d], and I. A. Al-Omari[e]

[a] *Ioffe Institute, St. Petersburg, Russia*
[b] *Department of Physics, United Arab Emirates University, Al-Ain 15551, United Arab Emirates*
[c] *Kazan Federal University, Kazan, Russia*
[d] *St. Petersburg State University, St. Petersburg, Russia*
[e] *Department of Physics, P.O. Box 36, Sultan Qaboos University, PC 123, Muscat, Sultanate of Oman*
**e-mail: ASKam@mail.ioffe.ru*

Received March 24, 2020; revised March 24, 2020; accepted June 15, 2020

Abstract—The composition and the magnetic structure of Fe_3O_4/γ-Fe_2O_3 nanoparticles placed into external magnetic field with a strength of 1.8 kOe are studied with Mössbauer spectroscopy. We showed that the thickness of the maghemite (γ-Fe_2O_3) shell can be changed by the synthesis conditions. We found that there is a layer, in which the magnetic moments are not oriented collinearly to those located in the depth of the shell, on the surface of maghemite (γ-Fe_2O_3) shell in the Fe_3O_4/γ-Fe_2O_3 nanocomposites; in other words, there is a canted spin structure. An intermediate layer in the spin-glass state is formed between the core and the shell. The data on structure of core/shell particles are important to understand the properties of nanocomposites, which are of great interest to apply in various fields, including biomedicine.

Keywords: magnetic nanoparticles, magnetic composites, core/shell, magnetic nanocomposites, biomedicine
DOI: 10.1134/S1063783420110153

1. INTRODUCTION

The use of magnetic nanoparticles in biomedicine [1, 2] requires the creation of new nanocomposites (NCs), for example, of a core/shell (C/S) type. The C/S NCs are more effective for cancer therapy with magnetic hyperthermia (MHT) [3, 4]. When MHT is used, the malignant cells die and the healthy one are not damaged under temperatures of 42–44°C [4–6]. The possibilities of using MNPs in theranostics, which combines the diagnostic and therapeutic methods, are being intensively studied [7, 8].

The magnetite (Fe_3O_4) is the most widely used in biomedicine among any other magnetic materials [4, 5]. Significant disadvantages of magnetite in biomedicine applications, however, are weak magnetic response and chemical instability. The magnetite particles may be covered with a protective surface layer to avoid these disadvantages of magnetite. It is known that natural oxidation of magnetite leads to the formation of a maghemite (γ-Fe_2O_3) layer on the surface of its particles Fe_3O_4 [9].

Maghemite as a protective layer not only enhances the chemical stability and the magnetic response of the Fe_3O_4/γ-Fe_2O_3 C/S NCs [10], but also does not worsen the biological compatibility [11–16]. In addition, high efficiency of heating the Fe_3O_4/γ-Fe_2O_3 C/S NCs with an external alternating magnetic field makes these materials much more attractive for hyperthermal treatment [15, 16]. Comprehensive studies of the magnetic structure of C/S NCs, however, are required, because the properties of such composites are mainly due to their magnetic structure.

Various techniques are used to study Fe_3O_4/γ-Fe_2O_3 C/S NCs to identify the phases of magnetite (Fe_3O_4) and maghemite (γ-Fe_2O_3) and to study the crystal and magnetic structures, phase states, distribution of NCs in size, and the degree of iron oxidation in them. An effective method to study NCs consisting of iron oxides is Mössbauer spectroscopy, which has a unique sensitivity to the local environment of Fe atoms in the crystal lattice and makes it possible to reliably distinguish the phases of iron oxides and hydroxides [17, 18], which is inaccessible to other methods.

The aim of this work is to continue the Mössbauer studies begun in [19] and to study the magnetic structure of Fe_3O_4/γ-Fe_2O_3 C/S NCs under external magnetic field of 1.8 kOe. Systematic studies of such C/S NCs are important from both fundamental and prac-

tical points of view, especially for biomedical applications.

2. EXPERIMENTAL

Fe_3O_4/γ-Fe_2O_3 NCs were synthesized via co-precipitation of Fe^{2+} and Fe^{3+} salts in aqueous media under strict control of a pH value and the ionic environment to control the size of particles and their size distribution as described in [16, 20]. The temperature was 80°C and the pressure was atmospheric during the synthesis. The Fe_3O_4/γ-Fe_2O_3 NCs, which had the same core diameter but different shell thicknesses, were obtained under these conditions.

The Fe_3O_4/γ-Fe_2O_3 NCs synthesized were characterized with various techniques [16, 20]. The structure of NCs being as C/S particles and consisting of Fe_3O_4 and γ-Fe_2O_3 was confirmed with a selected area electron diffraction (SAED) in our works [16, 20]. High-resolution transmission electron microscopy (HRTEM) data showed that the resulting NCs have an almost spherical shape. The histograms of particle size obtained with TEM indicated that the size distributions are narrow. The images obtained with HRTEM and SAED showed that the structure of NC particles is assigned to the C/S type [16, 20]. The studies [16, 20] showed that the thickness of NC shell depends on oxidation time of magnetite particles.

The Mössbauer measurements of Fe_3O_4/γ-Fe_2O_3 NCs were performed with the registration of gamma quanta from a Co^{57}(Rd) source in the geometry of transmission through the sample. The rate of Doppler displacement of the source relative to the sample was maintained in a constant acceleration mode and was calibrated with an α-Fe foil with 6 μm in thickness at room temperature. The Mössbauer measurements were performed for powders placed into a special plastic container to avoid additional oxidation of the NCs studied.

Experimental MS of Fe_3O_4/γ-Fe_2O_3 NCs were processed mathematically and the parameters of hyperfine interactions (HFIs) were calculated with a specialized program [21]. The discrepancy between the theoretical values of HFI parameters are found from statistical deviations [21]. The minimization procedure of a chi-square (χ^2) functional implies the search of optimal values of HFI parameters: the δ-isomeric shift of a Mössbauer line, the *QS*-quadrupole splitting, and the H_{eff} effective magnetic field.

3. RESULTS AND DISCUSSION

3.1. Mössbauer Spectra of Fe_3O_4/γ-Fe_2O_3 NCs at 300 K under External Magnetic Field and Their Analysis

The lines of Zeeman sextuplets on MS of Fe_3O_4/γ-Fe_2O_3 NCs acquired at room temperature [19] are broadened towards the center of the spectrum; as a result, it is difficult to separate dynamic effects resulting from relaxation phenomena from static ones, which are formed due to the particle size distribution. The Mössbauer spectra of Fe_3O_4/γ-Fe_2O_3 NCs were acquired under external magnetic field (EMF) of 1.8 kOe applied parallel to the direction of gamma radiation to distinguish these effects. Figure 1a shows the resulting MS. The designations *1H*, *2H*, and *3H* in it are assigned to the Fe_3O_4/γ-Fe_2O_3 NCs synthesized for 1, 2, and 3 h, respectively.

The experimental MS show only the Zeeman splitting lines, which indicate the magnetically ordered state of the particles studied. The fact that there are no broad Zeeman lines in MS, against the background of which there are no lines in the region of zero velocity indicating the presence of a paramagnetic phase in the samples, means that there is a rather narrow size distribution of the particles studied. In the case of relaxation behavior, the superposition of EMF of even a low strength should stabilize the relaxation processes, and the MS should contain the sufficiently well resolved Zeeman sextuplets. In the case of even low size distribution of the particles studied, the magnetic moments of iron ions should be oriented parallel to the direction of EMF, which leads to a decrease in intensities of the lines 2 and 5 (Fig. 1a). This evolution of the MS under EMF indicates that there are no relaxation effects in the Fe_3O_4/γ-Fe_2O_3 NCs and there is an insignificant particle size distribution.

Considering that magnetite and maghemite have a spinel structure, in which iron ions occupy two nonequivalent *A* and *B* crystallographic positions, the Mössbauer spectra should be a superposition of Zeeman sextuplets assigned to iron ions occupying these different crystallographic positions (*A* and *B*). Only two sextuplets in the MS of Fe_3O_4/γ-Fe_2O_3 NCs (Fig. 1a), however, were processed mathematically to simplify their analysis: one was assigned to magnetite Fe_3O_4 and the other one to maghemite. Such a model was in good agreement with the experimental data for NCs with the thinnest shell (Fig. 1a, *1H*). A third sextuplet was introduced to describe the Mössbauer spectra of NCs with thicker shells (Fig. 1a, *2H* and *3H*), so that this made it possible to obtain the best agreement between the models and experimental data. The model spectra obtained during the mathematical processing of the MS (Fig. 1a) with a specialized program [21] are shown as solid lines, and the experimental values are shown as dots. A good agreement between the models and the experimental spectra of Fe_3O_4/γ-Fe_2O_3 NCs is confirmed by the minimum differences between the model and experimental values shown above each spectrum (Fig. 1a) and the χ^2 values, which are within 1.0–1.2. Figure 1b shows the distribution functions of EMFs ($P(H_{\text{eff}})$) obtained from the MS of Fe_3O_4/γ-Fe_2O_3 NCs (Fig. 1a). Table 1 shows the HFI parameters calculated from the positions of Zeeman lines in the MS of Fe_3O_4/γ-Fe_2O_3 NCs.

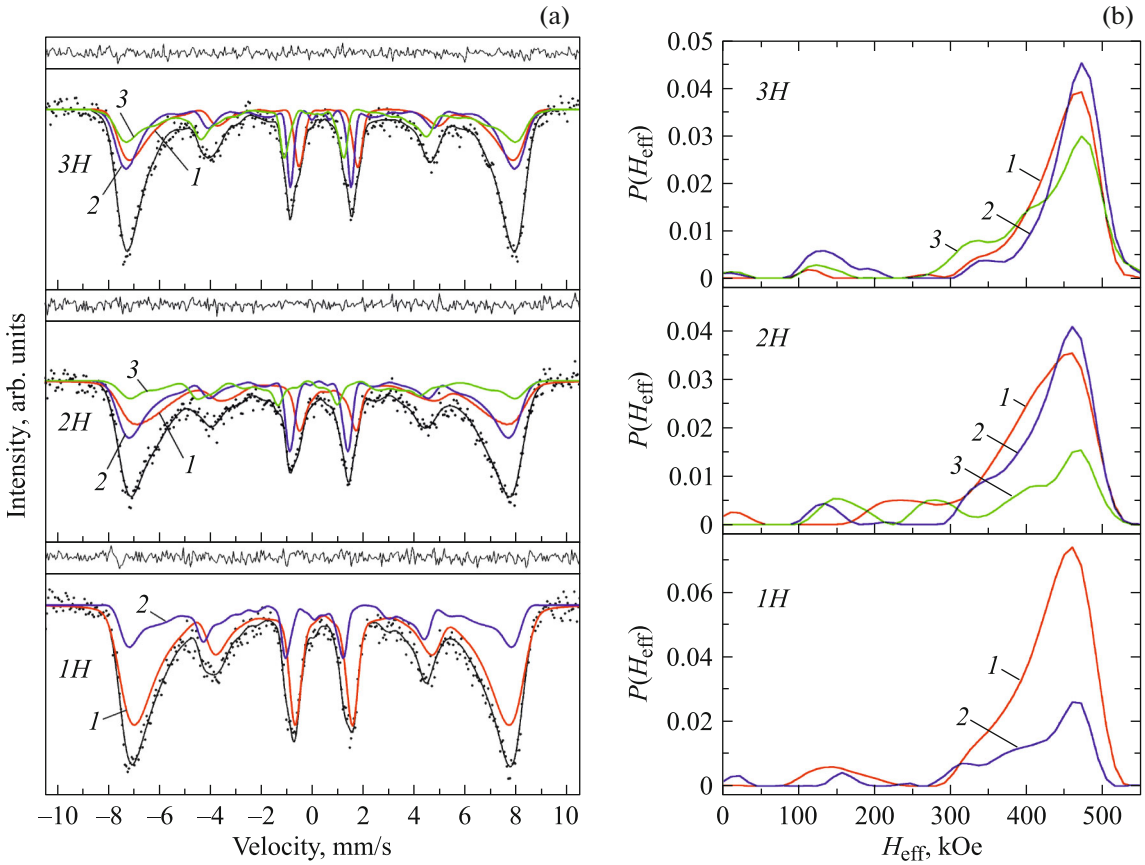

Fig. 1. Mössbauer spectra of Fe_3O_4/γ-Fe_2O_3 C/S NCs: (a) at 300 K under external magnetic field of 1.8 kOe applied parallel to the gamma-ray beam and (b) from distribution functions of effective magnetic fields $P(H_{eff})$. The difference between experimental and model values is shown above each spectrum. The designations *1H*, *2H*, and *3H* are assigned to samples synthesized for 1, 2, and 3 h, respectively. A sextuplet is assigned to: (*1*) Fe_3O_4, (*2*) γ-Fe_2O_3 shell in the case of *1H* sample and to the inner part of the shell in the case of *2H* and *3H* samples, and (*3*) the surface layer of the shell.

Table 1 shows that the fields H_{eff} for the components of the Fe_3O_4/γ-Fe_2O_3 NCs are lower than those for bulk crystals or for magnetite and maghemite nanoparticles [13, 22], which is due to the low sizes of the components of the NCs studied. The isomeric shifts (δ) and H_{eff} (Table 1) are characteristic of iron ions in the high-spin state (Fe^{3+}) and agree with the data for magnetite nanoparticles with sizes from 10 to 20 nm [22, 23]. The resulting δ and H_{eff} values are in good agreement with those for γ-Fe_2O_3 nanoparticles with sizes from 10 to 20 nm: $\delta = 0.42–0.44$ mm/s and $H_{eff} = 50–51$ T [24–29].

It is known that the EMFs (H_{eff}) on nuclei of iron ions in magnetite are lower than those in maghemite [17], but Table 1 shows that the H_{eff} value in magnetite under EMF is higher than that in maghemite. This is probably due to the different dependences of magnetization of a core and a shell on external field. In addition, the relationships between the blocking temperature and the external field for magnetite and maghemite are also different. We assume that both of these factors have an impact on H_{eff} values in the core and the shell.

The line intensities of Zeeman sextuplets in the Mössbauer spectra of magnets are as $3 : X : 1 : 1 : X : 3$ depending on orientation of the magnetic moments and the direction of EMF, where X is the intensities of the second or fifth lines. The β angle between the orientation of EMF and the direction of a gamma-ray beam parallel to the applied magnetic field is as follows [22, 30]:

$$\sin^2\beta = 6I/(4+3I), \quad (1)$$

where I is the intensity ratios of the second and first ($A2/A1$) or fifth and sixth ($A5/A6$) lines of the sextuplet.

The deviation angles from the EMF direction of the magnetic moments of iron ions located in the core (Fe_3O_4) of the Fe_3O_4/γ-Fe_2O_3 NCs calculated from Eqs. (1) are ~32°. The deviation angles of the moments located in the Fe_3O_4/γ-Fe_2O_3 NCs in the surface layer of the shell (γ-Fe_2O_3) are ~48°, whereas

Table 1. HFI parameters calculated from Mössbauer spectra of Fe_3O_4/γ-Fe_2O_3 C/S NCs obtained at 300 K under external magnetic field of 1.8 kOe applied parallel to the gamma-ray beam. Surf. s. is surface layer of shell in NCs, Compon. is components of NCs, *G* the widths of the first and sixth lines of sextuplets, δ the isomer shift, *QS* the quadrupole splitting, H_{eff} the effective magnetic field, and *S* the line area of each sextuplet in % of total area of spectrum. Isomeric shifts are given relative to α-Fe

Sample	Compon.	G, mm/s	δ, mm/s	*QS*, mm/s	H_{eff}, kOe	*S*, %
1H	Fe_3O_4	0.459 ± 0.090	0.384 ± 0.019	−0.040 ± 0.016	463.8 ± 1.6	71 ± 8
	γ-Fe_2O_3	0.325 ± 0.070	0.176 ± 0.029	0.118 ± 0.030	458.4 ± 2.1	29 ± 8
2H	Fe_3O_4	0.319 ± 0.080	0.262 ± 0.032	0.001 ± 0.032	461.2 ± 2.3	43 ± 3
	γ-Fe_2O_3	0.330 ± 0.150	0.505 ± 0.050	−0.111 ± 0.040	466.7 ± 5.0	
	Surf. s.	0.312 ± 0.160	0.120 ± 0.070	0.287 ± 0.070	476.1 ± 4.0	57 ± 2
3H	Fe_3O_4	0.234 ± 0.050	0.310 ± 0.034	−0.009 ± 0.032	471.9 ± 1.7	31 ± 12
	γ-Fe_2O_3	0.348 ± 0.090	0.478 ± 0.040	−0.140 ± 0.040	477.5 ± 2.2	
	Surf. s.	0.233 ± 0.090	0.188 ± 0.060	0.134 ± 0.060	472.3 ± 2.1	69 ± 16

the magnetic moments of Fe ions located far from the shell surface (γ-Fe_2O_3) are ~30°. As a result, there is a layer on the surface of the shell of Fe_3O_4/γ-Fe_2O_3 NCs, in which the magnetic moments form a certain angle with those located in the depth of the shell. In other words, the magnetic moments in the surface layer and in the depth of the shell are oriented noncollinear to each other. Figure 2 shows a schematic representation of the structure of the core and the shell of the Fe_3O_4/γ-Fe_2O_3 NCs.

The fact that there was no complete ordering of the magnetic moments in γ-Fe_2O_3 nanoparticles along the direction even under strong external magnetic field (up to 5 T) was described earlier [32] with Mössbauer spectroscopy. This noncollinearity of the spin structure of the surface layer and the volume of nanoparticles is due to the competing antiferromagnetic exchange interactions, which are most possible on the particle surface. The magnetic ions located on the surface of particles have fewer magnetic ions in their nearest neighbors than the nanoparticles located in the bulk. This can lead to a weakening of magnetic

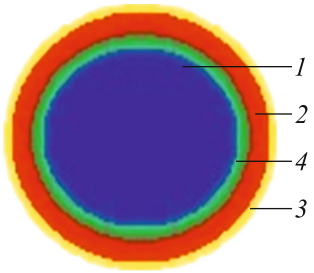

Fig. 2. Schematic representation of Fe_3O_4/γ-Fe_2O_3 NCs. (*1*) Fe_3O_4 core, (*2*) the inner part of γ-Fe_2O_3 shell, (*3*) the surface layer of shell with a canted spin structure, and (*4*) the layer intermediate between core and shell in spin-glass phase.

interactions and to a skew of magnetic moments in the surface layer of the particle relative to the orientation of the moments in the volume of the particle. Low local symmetry near the surface can lead to a large contribution to the local magnetic anisotropy, which can also affect the orientation of spin moments. The results in [31] also explain why the saturation magnetization in the systems of nanoparticles is lower than that in a bulk crystal. A skewed structure of spin moments was observed in the surface layer of other oxides [32–35].

The maximum observed within ~340–460 kOe on the $P(H_{eff})$ distribution functions for an additional sextuplet (Fig. 1b) obtained from experimental MS of Fe_3O_4/γ-Fe_2O_3 NCs at 300 K under external magnetic field (Fig. 1a) is due to iron ions located in the depth from the shell surface (440 kOe) and having the total number of magnetic neighbors. It is also due to iron ions occupying the positions on the shell surface and not having half of the nearest magnetic neighbors, which leads to a decrease in H_{eff} up to 360 kOe.

The maximum observed within ~120–160 kOe on the function $P(H_{eff})$ (Fig. 1b) is probably due to the fact that a spin-glass state appears in the intermediate layer between the core and the shell [36, 37], in which the effective magnetic fields significantly lower than that in a material with a crystalline structure.

4. CONCLUSIONS

The composition and the magnetic structure of Fe_3O_4/γ-Fe_2O_3 nanocomposites (NCs) were studied systematically. Monodisperse Fe_3O_4/γ-Fe_2O_3 core/shell (C/S) NCs were synthesized via co-precipitation by controlling the temperature and the time of oxidation of the core. We found that three types of C/S NCs formed from the core of the same size from magnetite (Fe_3O_4) and covered with a shell of different

thickness from maghemite (γ-Fe_2O_3) were synthesized. No any other phases were found.

We found that there is a thin layer on the shell surface, in which the magnetic moments of Fe ions are oriented at an angle relative to the direction of the moments in the inner part of the shell. In other words, a thin layer with a spin structure skewed relative to the moments in the depth of the shell appears on the shell surface. This leads to a high magnetic anisotropy of the γ-Fe_2O_3 shell and, probably, to the exchange bias in the $M(H)$ curves. An intermediate layer being in the spin-glass phase was found between the shell and the core.

Important data were obtained for the first time from Mössbauer studies for magnetic structure of Fe_3O_4/γ-Fe_2O_3 C/S NCs, for the differences in the magnetic structure of the surface and inner layers of the shell, and the structure of the layer intermediate between the core and the shell. The data obtained will make it possible to explain the magnetic properties and effects of exchange bias in nanostructures of a core/shell type, which is important to develop and to obtain magnetic NCs for various applications, including biomedicine.

FUNDING

I.M. Obaidat and I.A. Al-Omari are grateful for the financial support of the UAEU Advanced Research Program (UPAR), grant no. 31S241.

CONFLICT OF INTEREST

The authors declare that they have no conflicts of interest.

REFERENCES

1. *Nanoparticles for Biomedical Applications: Fundamental Concepts, Biological Interactions and Clinical Applications*, Ed. by Eun Ji Chung, L. Leon, and C. Rinaldi (Elsevier, Amsterdam, 2019).
2. *Hybrid Nanostructures for Cancer Theranostics*, Ed. by R. Ashok Bohara and N. Thorat (Elsevier, Amsterdam, 2019).
3. F. Fabris, E. Lima, Jr., E. de Biasi, H. E. Troiani, M. Vásquez Mansilla, T. E. Torres, R. Fernández Pacheco, M. Ricardo Ibarra, G. F. Goya, R. D. Zysler, and E. L. Winkler, Nanoscale **11**, 3164 (2019).
4. I. M. Obaidat, V. Narayanaswamy, S. Alaabed, S. Sambasivam, and Ch. V. V. Muralee Gopi, Magnetochemistry **5**, 67 (2019).
5. Y. H. Byun, H. Sh. Gwak, J.-W. Kwon, M. K. Song, S. H. Shin, Y. H. Jo, H. Yoo, and S. H. Lee, Int. J. Hypertherm. **35**, 168 (2018).
6. K. Mahmoudi, A. Bouras, D. Bozec, R. Ivkov, and C. Hadjipanayis, Int. J. Hypertherm. **34**, 1316 (2018).
7. Yu. I. Golovin, N. L. Klyachko, A. G. Mazhuga, S. L. Gribanovskii, D. Yu. Golovin, A. O. Zhigachev, A. V. Shuklinov, M. V. Efremova, M. M. Veselov, K. Yu. Vlasova, A. D. Usvaliev, I. M. Le-Deygen, and A. V. Kabanov, Nanotechnol. Russ. **13**, 215 (2018).
8. W. Xie, Zh. Guo, F. Gao, Q. Gao, D. Wang, B.-sh. Liaw, Q. Cai, X. Sun, X. Wang, and L. Zhao, Theranostics **8**, 3284 (2018).
9. U. Colombo, G. Fagherazzi, S. Gazzarrini, G. Lanzavecchia, and G. Sroni, Nature (London, U.K.) **219**, 1036 (1968).
10. D-E. Lee, H. Koo, I-C. Sun, J. N. Ryu, K. Kim, and I. C. Kwon, Chem. Soc. Rev. **41**, 2656 (2012).
11. Sh.-Ch. Lee, Ch.-M. Fu, and F.-H. Chang, Appl. Phys. Lett. **103**, 163104 (2013).
12. A. V. Bykov, V. I. Nikolaev, E. Reguera Ruiz, Yu. Ya. Kharitonov, O. G. Cherkasova, and V. I. Shulgin, Hyperfine Interact. **67**, 603 (1991).
13. M. Starowicz, P. Starowicz, J. Zukrowski, J. Przewoznik, A. Lemanski, C. Kapusta, and J. Banas, J. Nanopart. Res. **13**, 7167 (2011).
14. H. Sharifi Dehsari, V. Ksenofontov, A. Möller, G. Jakob, and K. Asadi, J. Phys. Chem. C **122**, 28292 (2018).
15. O. M. Lemine, *Hybrid Nanostructures for Cancer Theranostics, Micro and Nano Technologies* (Elsevier, Amsterdam, 2019), Chap. 7, p. 125.
16. I. M. Obaidat, Ch. Nayek, K. Manna, G. Bhattacharjee, I. A. Al-Omari, and A. Gismelseed, Nanomaterials **7**, 415 (2017).
17. A. S. Kamzin and N. Wakiya, Phys. Solid State **60**, 2608 (2018).
18. A. S. Kamzin, H. Das, N. Wakiya, and A. A. Valiullin, Phys. Solid State **60**, 1752 (2018).
19. A. S. Kamzin, I. M. Obaidat, A. A. Valliulin, V. G. Semenov, and I. A. Al-Omari, Phys. Solid State **62**, 1933 (2020).
20. I. M. Obaidat, Ch. Nayek, and K. Manna, Appl. Sci. **7**, 1269 (2017).
21. M. E. Matsnev and V. S. Rusakov, AIP Conf. Proc. **1489**, 178 (2012).
22. E. Murad and J. H. Johnston, in *Mössbauer Spectroscopy Applied to Inorganic Chemistry*, Ed. by G. J. Long (Plenum, New York, 1987), Vol. 2.
23. I. N. Zakharova, M. A. Shipilin, V. P. Alekseev, and A. M. Shipilin, Tech. Phys. Lett. **38**, 55 (2012).
24. L. Häggström, S. Kamali, T. Ericsson, P. Nordblad, A. Ahniyaz, and L. Bergström, in *Proceedings of the 29th International Conference on the Applications of the Mössbauer Effect (ICAME 2007), Kanpur, India, October 14–19, 2007.*
25. R. E. Vandenberghe and E. de Grave, in *Mössbauer Spectroscopy Applied to Inorganic Chemistry*, Ed. by G. J. Long and F. Grandjean (Plenum, New York, 1989), Vol. 3.
26. E. Lima, A. L. Brandl, A. D. Arelaro, and G. F. Goya, J. Appl. Phys. **99**, 083908 (2006).
27. S. Brice-Profeta, M.-A. Arrio, E. Tronc, N. Menguy, I. Letard, C. Cartier dit Moulin, M. Noguès, C. Chaneác, J.-P. Jolivet, and P. Sainctavit, J. Magn. Magn. Mater. **288**, 354 (2005).
28. R. R. Gabbasov, V. M. Cherepanov, M. A. Chuev, M. A. Polikarpov, and V. Y. Panchenko, Hyperfine Interact. **226**, 383 (2014).

29. M. Siddique, N. Hussain, and M. Shafi, J. Mater. Sci. Technol. **25**, 479 (2009).

30. A. S. Kamzin and L. P. Ol'khovik, Phys. Solid State **41**, 1658 (1999).

31. J. M. D. Coey, Phys. Rev. Lett. **27**, 1140 (1971).

32. A. E. Berkowitz, J. A. Lahut, I. S. Jacobs, L. M. Levinson, and D. W. Forester, Phys. Rev. Lett. **340**, 594 (1975).

33. K. Haneda, H. Kojima, A. H. Morrish, P. I. Picone, and K. Wakai, J. Appl. Phys. **53**, 2686 (1982).

34. S. Linderoth, P. V. Hendriksen, F. Bodker, S. Wells, K. Davies, and S. W. Charles, J. Appl. Phys. **75**, 6583 (1994).

35. P. V. Hendriksent, S. Linderotht, C. A. Oxborrow, and S. Mgrup, J. Phys.: Condens. Matter **6**, 3091 (1994).

36. K. Nadeem, H. Krenn, T. Traussing, and I. Letofsky-Papst, J. Appl. Phys. **109**, 013912 (2011).

37. R. Topkaya, O. Akman, S. Kazan, B. Aktas, Z. Durmus, and A. Baykal, J. Nanopart. Res. **14**, 1156 (2012).

Translated by A. Tulyabaev